

# Measuring the sampling coherence of a terahertz quantum cascade laser

Jean Maysonave,<sup>1</sup> Nathan Jukam,<sup>1,2,\*</sup> M. Shahrizan M. Ibrahim,<sup>3</sup> Rakchanok Rungswang,<sup>1</sup> Kenneth Maussang,<sup>1</sup> Julien Madéo,<sup>1</sup> Pierrick Cavalié,<sup>1</sup> Paul Dean,<sup>3</sup> Suraj P. Khanna,<sup>3</sup> D. Paul Steenson,<sup>3</sup> Edmund H. Linfield,<sup>3</sup> A. Giles Davies,<sup>3</sup> Sukhdeep S. Dhillon,<sup>1</sup> and Jérôme Tignon<sup>1</sup>

<sup>1</sup>Laboratoire Pierre Aigrain, Ecole Normale Supérieure, CNRS (UMR 8551), Université P. et M. Curie, Université D. Diderot, 75231 Paris Cedex 05, France

<sup>2</sup>Fakultät für Physik und Astronomie, Ruhr-Universität Bochum, Universitätsstraße 150, 44780 Bochum, Germany

<sup>3</sup>School of Electronic and Electrical Engineering, University of Leeds, Woodhouse Lane, Leeds LS9 2JT, UK  
[\\*nathan.jukam@rub.de](mailto:nathan.jukam@rub.de)

**Abstract:** The emission of a quantum cascade laser can be synchronized to the repetition rate of a femtosecond laser through the use of coherent injection seeding. This synchronization defines a sampling coherence between the terahertz laser emission and the femtosecond laser which enables coherent field detection. In this letter the sampling coherence is measured in the time-domain through the use of coherent and incoherent detection. For large seed amplitudes the emission is synchronized, while for small seed amplitudes the emission is non-synchronized. For intermediate seed amplitudes the emission exhibits a partial sampling coherence that is time-dependent.

©2012 Optical Society of America

**OCIS codes:** (040.2235) Far infrared or terahertz; (140.3070) Infrared and far-infrared lasers; (140.5965) Semiconductor lasers, quantum cascade; (320.7080) Ultrafast devices.

---

## References and links

1. D. H. Auston, A. M. Johnson, R. R. Smith, and J. C. Bean, "Picosecond optoelectronic detection, sampling, and correlation measurements in amorphous semiconductors," *Appl. Phys. Lett.* **37**(4), 371–373 (1980).
2. M. van Exter, Ch. Fattinger, and D. Grischkowsky, "High brightness terahertz beams characterized with an ultrafast detector," *Appl. Phys. Lett.* **55**(4), 337–339 (1989).
3. J. A. Valdmanis, G. Mourou, and C. W. Gabel, "Picosecond electro-optic sampling system," *Appl. Phys. Lett.* **41**(3), 211–212 (1982).
4. A. Nahata, A. S. Weling, and T. F. Heinz, "A wideband coherent terahertz spectroscopy system using optical rectification and electro-optic sampling," *Appl. Phys. Lett.* **69**(16), 2321–2323 (1996).
5. J. Dai, X. Xie, and X. C. Zhang, "Detection of broadband terahertz waves with a laser-induced plasma in gases," *Phys. Rev. Lett.* **97**(10), 103903 (2006).
6. D. H. Auston and K. P. Cheung, "Coherent time-domain far-infrared spectroscopy," *J. Opt. Soc. Am. B* **2**(4), 606–612 (1985).
7. C. A. Schmuttenmaer, "Exploring dynamics in the far-infrared with terahertz spectroscopy," *Chem. Rev.* **104**(4), 1759–1780 (2004).
8. P. Gaal, M. B. Raschke, K. Reimann, and M. Woerner, "Measuring the optical frequencies in the 0–40 THz range with non-synchronized electro-optic sampling," *Nat. Photonics* **1**(10), 577–580 (2007).
9. Z. Jiang and X. C. Zhang, "Single-shot spatiotemporal terahertz field imaging," *Opt. Lett.* **23**(14), 1114–1116 (1998).
10. R. A. Cheville and D. Grischkowsky, "Far-infrared terahertz time-domain spectroscopy of flames," *Opt. Lett.* **20**(15), 1646–1648 (1995).
11. J. Kröll, J. Darmo, S. S. Dhillon, X. Marcadet, M. Calligaro, C. Sirtori, and K. Unterrainer, "Phase-resolved measurements of stimulated emission in a laser," *Nature* **449**(7163), 698–701 (2007).
12. N. Jukam, S. S. Dhillon, D. Oustinov, Z.-Y. Zhao, S. Hameau, J. Tignon, S. Barbieri, A. Vasanelli, P. Filloux, C. Sirtori, and X. Marcadet, "Investigation of spectral gain narrowing in quantum cascade lasers using terahertz time domain spectroscopy," *Appl. Phys. Lett.* **93**(10), 101115 (2008).
13. D. Burghoff, T.-Y. Kao, D. Ban, A. W. M. Lee, Q. Hu, and J. Reno, "A terahertz pulse emitter monolithically integrated with a quantum cascade laser," *Appl. Phys. Lett.* **98**(6), 061112 (2011).
14. B. S. Williams, "Terahertz quantum cascade lasers," *Nat. Photonics* **1**(9), 517–525 (2007).

15. D. Oustinov, N. Jukam, R. Rungsawang, J. Madéo, S. Barbieri, P. Filloux, C. Sirtori, X. Marcadet, J. Tignon, and S. Dhillon, "Phase seeding of a terahertz quantum cascade laser," *Nat. Commun.* **1**(6), 69 (2010).
16. S. Barbieri, M. Ravaro, P. Gellie, G. Santarelli, C. Manquest, C. Sirtori, S. P. Khanna, E. H. Linfield, and A. G. Davies, "Coherent sampling of active mode-locked terahertz quantum cascade lasers and frequency synthesis," *Nat. Photonics* **5**(5), 306–313 (2011).
17. G. Scalari, M. I. Amanti, C. Walther, R. Terazzi, M. Beck, and J. Faist, "Broadband THz lasing from a photon-phonon quantum cascade structure," *Opt. Express* **18**(8), 8043–8052 (2010).
18. C. Y. Wang, L. Kuznetsova, V. M. Gkortsas, L. Diehl, F. X. Kärtner, M. A. Belkin, A. Belyanin, X. Li, D. Ham, H. Schneider, P. Grant, C. Y. Song, S. Haffouz, Z. R. Wasilewski, H. C. Liu, and F. Capasso, "Mode-locked pulses from mid-infrared quantum cascade lasers," *Opt. Express* **17**(15), 12929–12943 (2009).
19. A. Dreyhaupt, S. Winnerl, T. Dekorsy, and M. Helm, "High-intensity terahertz radiation from a microstructure large-area photoconductor," *Appl. Phys. Lett.* **86**(12), 121114 (2005).
20. N. Jukam, S. S. Dhillon, D. Oustinov, J. Madeo, C. Manquest, S. Barbieri, C. Sirtori, S. P. Khanna, E. H. Linfield, A. G. Davies, and J. Tignon, "Terahertz amplifier based on gain switching in a quantum cascade laser," *Nat. Photonics* **3**(12), 715–719 (2009).
21. J. Maysonnave, N. Jukam, M. S. M. Ibrahim, K. Maussang, J. Madéo, P. Cavalié, P. Dean, S. P. Khanna, D. P. Steenson, E. H. Linfield, A. G. Davies, J. Tignon, and S. S. Dhillon, "Integrated injection seeded terahertz source and amplifier for time-domain spectroscopy," *Opt. Lett.* **37**(4), 731–733 (2012).
22. R. Rungsawang, O. Marshall, J. R. Freeman, H. E. Beere, S. Malik, J. Alton, S. Barbieri, and D. A. Ritchie, "Intensity detection of terahertz quantum cascade laser radiation using electro-optic sampling," *Appl. Phys. Lett.* **93**(19), 191111 (2008).
23. J. Darmo, M. Martl, and K. Unterrainer, "Quasi phase-matched terahertz detector," *Electron. Lett.* **46**(11), 788–790 (2010).
24. Z. Jiang, F. G. Sun, Q. Chen, and X. C. Zhang, "Electro-optic sampling near zero-transmission point," *Appl. Phys. Lett.* **74**(9), 1191–1193 (1999).
25. G. Gallot, J. Zhang, R. W. McGowan, T. I. Jeon, and D. Grischkowsky, "Measurement of the THz absorption and dispersion of ZnTe and their relevance to the electro-optic detection of THz radiation," *Appl. Phys. Lett.* **74**(23), 3450–3452 (1999).

## 1. Introduction

A femtosecond laser pulse can measure (or sample) the phase-resolved value of a terahertz (THz) electric field by using techniques such as photo-conductive sampling [1,2], electro-optic detection [3,4], and air-plasma sampling [5]. The sampling of THz fields with femtosecond pulses is often referred to as coherent detection in the literature [6], and depends on the absence of timing jitter (i.e. perfect synchronization between the THz pulses and the femtosecond pulses). If the femtosecond and THz pulses are synchronized with respect to each other, a large number of sampling events can be summed coherently without adding different phase values. Time-resolved measurements of the THz fields can be achieved by changing the delay time between the femtosecond and the THz pulse with an optical delay line. By transforming the field into the frequency domain, the spectral amplitude and phase can be recovered. As a result THz time-domain spectroscopy (TDS) is a widely used technique to investigate phenomena at THz frequencies [7].

In contrast, if the THz pulses are not synchronized with the femtosecond laser, successive femtosecond pulses will sample different parts of the successive THz pulses, and the sum of a large number of sampling events will approach zero. The standard deviation of non-synchronous sampling events can be significant; this can enable frequency information to be retrieved [8]. And if the THz field and signal are strong enough, single shot phase-resolved measurements can also be made [9]. However, in typical experimental arrangements, a large number of sampling events takes place, and this prevents phase-resolved detection of non-synchronized THz signals. The inability to detect non-synchronized radiation can be an advantage when a strong background signal must be removed [10]. For example coherent THz detection can be used to probe the gain [11–13] of THz quantum cascade lasers (QCLs) [14] without detecting the non-synchronized laser emission of the QCL.

Sampling coherence can be defined as the correlation (i.e. synchronization) between the THz pulse and the sampling femtosecond pulses which permits coherent detection. Traditionally THz sources have exhibited either complete sampling coherence (e.g. THz femtosecond based sources) or incomplete sampling coherence (e.g. thermal sources).

However, recently, THz QCLs were synchronized to femtosecond lasers using coherent injection seeding [15] and a feedback stabilization/injection locking scheme [16]. This enabled coherent detection of the phase-resolved emission from a QCL in the time domain and presents the possibility of using QCLs as sources for THz TDS. Although QCLs are sources of bright, narrow-band THz radiation, QCLs can also be designed with ultra-large gain bandwidths [17] and mode-locked for short pulse formation [16, 18]. However, in contrast to other THz sources QCLs may exhibit partial sampling coherence, in addition to complete and incomplete sampling coherence. If QCLs are to realize their full potential as synchronized THz sources, diagnostic measurements of the sampling coherence must be developed preferably in the time-domain.

In this letter, we measure the degree of sampling coherence between a QCL and a femtosecond laser. (The femtosecond laser triggers coherent THz pulses that injection seed the QCL.) The sampling coherence is measured by using electro-optic sampling in two different configuration geometries to record the synchronized THz field component and the envelope of the instantaneous THz intensity (which includes both synchronized and non-synchronized components). This permits the sampling coherence to be measured on picosecond time scales.

## 2. Synchronized field measurements in the quarter wave geometry

The QCL is based on a bound-to-continuum design with a single plasmon waveguide (length 2.85mm) that shows laser action at 2.5THz. All measurements are taken at 10K. THz seed pulses are generated by illuminating an inter-digitated photoconductive antenna [19] with femtosecond laser pulses. An RF pulse is produced by illuminating a fast photodetector with a portion of the femtosecond laser beam. The RF pulses are subsequently amplified with a GaN power amplifier (with a nominal bandwidth of 20MHz-6GHz, and a saturation power of 10W) before they are sent to the QCL. The THz seed pulse is coupled into the QCL cavity while an RF electrical pulse drives the QCL bias above threshold as shown in Fig. 1(a). This places the QCL in a transitory state where the gain can be greater than the losses and large amplification can occur [20]. Both the QCL spontaneous emission and the injected THz seed pulse are amplified until the internal THz field is strong enough to saturate the QCL gain and clamp it to the total losses. Since the THz seed is phase-locked to the femtosecond laser, emission originating from the THz seed is synchronized and can be detected in the quarter-wave geometry. In contrast emission originating from amplified spontaneous emission (ASE) in the QCL has a random phase, and cannot be detected in the quarter-wave geometry since it is not synchronized to the femtosecond laser.

The synchronized field measured in the quarter-wave geometry [4] is shown in Fig. 1(c). The THz seed pulses undergo multiple passes through the QCL cavity, which correspond to reflections of the THz pulse at the ends of the cavity. Initially the pulses are amplified as the RF pulse turns on the QCL. After ~150ps the amplitude of the THz output pulses (at the cavity round-trip time of ~70ps) are more or less constant, and remains so for ~400ps which corresponds to the duration of the RF pulse as shown in Fig. 1(b). (Besides the primary seed pulse at ~0ps which occur at the round-trip time, secondary seed pulses arises from reflections in the photoconductive antenna substrate. Without the secondary seed pulses the QCL emission would only consist of the primary pulses separated by the round-trip time [21].)

Figure 1(d) shows the amplitude of the fourth, fifth, sixth and seventh THz pulses as a function of the antenna bias voltage, which is proportional to the amplitude of the THz input pulse [15]. The amplitude of the THz output pulse saturates as the amplitude of the input THz seed pulse increases. This implies that the amplified seed pulse (generated with an antenna bias of 4.0V) in Fig. 1(c) saturates the QCL gain, and indicates any non-synchronized field component in Fig. 1(c) is small at the fourth, fifth, sixth, and seventh round-trip times. However, at other times between the round trip pulses such as 341.5ps, which is shown in Fig. 1(e), no synchronized field is present. Incoherent measurements of the intensity-envelope in

the cross-polarizer geometry are then necessary to determine if a non-synchronized field component is present at these times.

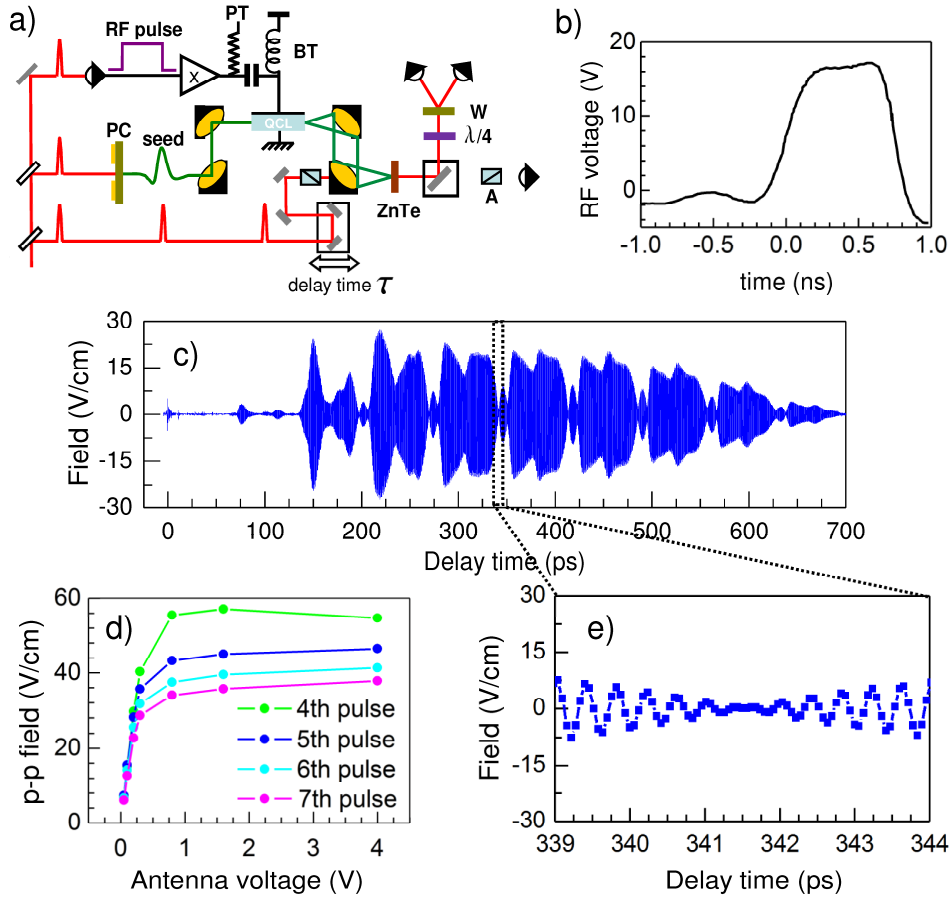


Fig. 1. **a)** RF pulses bias the QCL along with a quasi-DC bias added with a bias tee (BT). THz seed pulses (generated from a photoconductive antenna [PC]) are coupled into a facet of the QCL. The output from the opposite facet is focused onto a ZnTe crystal for electro-optic detection, which takes place in either a quarter-wave geometry with  $\lambda/4$  wave-plate and Wollaston prism (W), or a cross-polarizer geometry with an analyzer (A). The detection geometry can be changed by moving a mirror on a translation stage. **b)** The RF pulse measured with a pick-off tee (PT). The zero position is approximate and cannot be calibrated with the zero position of the femtosecond delay line. **c)** The synchronized THz field of the injection seeded QCL measured in the quarter-wave geometry. A quasi-DC bias of (1.91V, 70 A/cm<sup>2</sup>) is applied to the QCL, which is significantly less than the threshold bias (3.21V, 125 A/cm<sup>2</sup>) and the maximum QCL power bias (3.63V, 157 A/cm<sup>2</sup>). A 6W RF pulse, which experiences a significant reflection from the impedance mismatch of the QCL, drives the QCL above threshold to roughly the maximum QCL power bias. The photoconductive antenna is biased at 4V. **d)** Maximum peak-to-peak (p-p) THz field of the fourth, fifth, sixth, and seventh round-trip pulses in part **c)** as a function of the THz antenna bias voltage, which is proportional to the seed amplitude. **e)** A portion of part **c)**, for which the synchronized THz field approaches zero.

### 3. Measurement of the total emission of the QCL in the cross polarizer geometry

Electro-optic sampling in the cross-polarizer geometry has an intensity response that can be used to measure the power emission of a non-synchronized QCL [22, 23]. However detection in the cross-polarizer geometry also contains a strong amplitude response that is typically much greater than the intensity response [24]. In this work the amplitude response is completely removed from the cross polarizer signal by using a fast scan and antenna

modulation technique described in the Appendix. This allows the instantaneous intensity-envelope of the QCL emission to be measured even in the presence of a strong synchronized THz field which would normally dominate the signal of the cross-polarizer measurement.

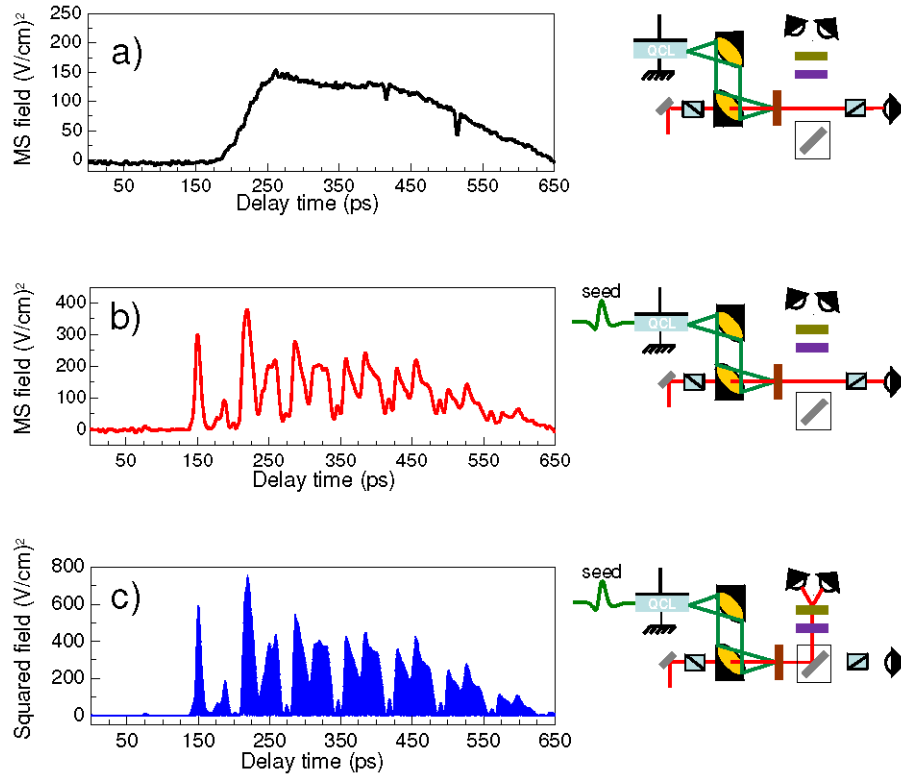


Fig. 2. The mean square (MS) field-envelope of the total emission (synchronized and non-synchronized) of the QCL measured in the cross-polarizer geometry in the absence of a THz seed pulse **a**) and with a THz seed pulse **b**). For part **b** an antenna bias of 4.0V is used to generate the seed. **c**) The square of the phase-resolved synchronized field measured in the quarter-wave geometry, with a 4.0V THz antenna bias. The time scale is too large to discern the individual field oscillations. (The MS field envelope is half the maximum value of the squared field.) For all graphs the RF power is 6W, and the quasi-DC bias is 1.91V - 70A/cm<sup>2</sup>.

When the RF pulse is applied in the absence of the THz seed in Fig. 2(a); lasing action is initiated by ASE; all phase information is lost; and only the mean square of the envelope of the field (MS field-envelope) is constant from pulse to pulse. The shape of the MS field-envelope when the QCL is seeded, which is shown in Fig. 2(b), is considerably different than the shape of the MS field-envelope when the QCL is not seeded. In Fig. 2(b) laser action is initiated by the THz seed pulse, and QCL emission begins at a significantly earlier time due to the large amplitude of the initial seed pulse. In contrast to the non-seeded emission in Fig. 2(a), the seeded emission in Fig. 2(b) consists of several peaks separated by the round-trip time. The maximum field of the seeded emission is 2.6 times larger than that of the non-seeded emission. The peaks of the synchronized squared field in Fig. 2(c), which are obtained from the data in Fig. 1(c), correspond perfectly with peaks of the MS field-envelope in Fig. 2(b) which indicates that a significant portion of the QCL emission is synchronized to the femtosecond laser.

#### 4. Measuring the sampling coherence in the time-domain

For coherent detection in the quarter-wave geometry the sampled field,  $E_s(\tau)$ , can be expressed as the cross-correlation between the envelope of the femtosecond laser power,  $P_{fs}(t - \tau)$  and the actual THz electric field,  $E_{THz}(t)$  as

$$E_s(t) = \left( \frac{1}{J_{fs}L} \right) \int_0^{LT} P_{fs}(t-\tau) E_{THz}(t) dt ; \frac{P_{fs}(t-\tau)}{J_{fs}} \approx \sum_{n=0}^L \delta(t-nT). \quad (1)$$

In Eq. (1)  $\tau$  is the time delay introduced by the optical delay line,  $t$  is the laboratory time,  $T$  is the period of the femtosecond pulses,  $J_{fs}$  is average integrated power of each laser pulse, and  $L$  is the number of femtosecond pulses in the measurement, which is typically a very large number. If the duration of the laser pulse is much less than the period of the THz wave, the laser pulses can be approximated as a train of Dirac delta functions. Equation (1) assumes ideal electro-optic sampling and does not take account of phase matching, absorption, or any frequency dependence of the electro-optic coefficient. If the THz field is not correlated with the femtosecond pulse the sampled THz field will go to zero as the number of samples ( $L$ ) increases. Coherent detection in the quarter wave geometry is thus not only a measure of the THz field strength, but also a measure of the mutual correlation between the QCL and the femtosecond laser, which is the sampling coherence. Sampling coherence is a distinct concept from temporal coherence, since temporal coherence is determined by the self-correlation  $\left( \int E_{THz}(t-\tau) E_{THz}(t) dt \right)$  of the THz field. The degree of sampling coherence,  $\gamma_s(\tau)$ , can be defined as the ratio of the envelope function of the sampled field to the envelope function of the actual field. (Note that if the sampling coherence were defined in terms of the fields,  $\gamma_s(\tau)$  would oscillate with the phase of the THz frequency. The envelope function of the MS synchronized field can be calculated by mathematically filtering out the high frequency oscillations in the synchronized squared field.) If  $\gamma_s(\tau) = 1$  the femtosecond laser and THz radiation are perfectly synchronized, while if  $\gamma_s(\tau) = 0$  there is no synchronization between the THz emission and the femtosecond laser.

The sampling coherence depends on the amplitude of the injected seed pulse as shown in Fig. 3. For the smallest THz seed pulse, shown in Figs. 3(a) and 3(e), the QCL emission is predominantly non-synchronized,  $\gamma_s \sim 0$ . Here the amplitude of the seed pulse is significantly less than the RMS of the spontaneous emission, and the majority of QCL emission arises from ASE. The amplified THz pulses are proportional to the input pulse. This linear amplification regime corresponds to the lowest seed amplitudes (or THz antenna biases) of the saturation curve in Fig. 1(d). For larger THz seed pulses, the QCL emission exhibits partial sampling coherence, as shown in Figs. 3(b) and 3(c). THz sources are often assumed to be either completely synchronized ( $\gamma_s = 1$ ) or non-synchronized ( $\gamma_s = 0$ ) with respect to the femtosecond laser, but Figs. 3(f) and 3(g) show that this is not always true. In addition the sampling coherence is maximized for delay times that correspond to an integer number of round-trips of the seed pulse. This demonstrates that partial sampling coherence cannot be completely characterized by integrated time-average measurements of the synchronized and non-synchronized power. For the largest THz seed amplitude, shown in Figs. 3(d) and 3(h), the QCL emission is predominately synchronized with the femtosecond laser, except for times where the total emission is very small. This is the injection seeding regime where the amplitude of the seed pulse is significantly greater than the RMS field of the spontaneous emission. In this regime the THz seed initiates lasing and saturates the QCL gain. In Fig. 3(d), 98% of the integrated THz power is synchronized with the femtosecond laser, which indicates the majority of the QCL power originates from the amplified seed pulse. (The artifact from 162 to 175ps in Fig. 3(h) is due to the low MS-field values at these times. Unexplained drops

in the cross polarizer signal in Fig. 2(a) are present at 415ps and 515ps, and the artifact near 570ps in Fig. 3(h) is probably due to a similar drop in the cross polarizer signal.)

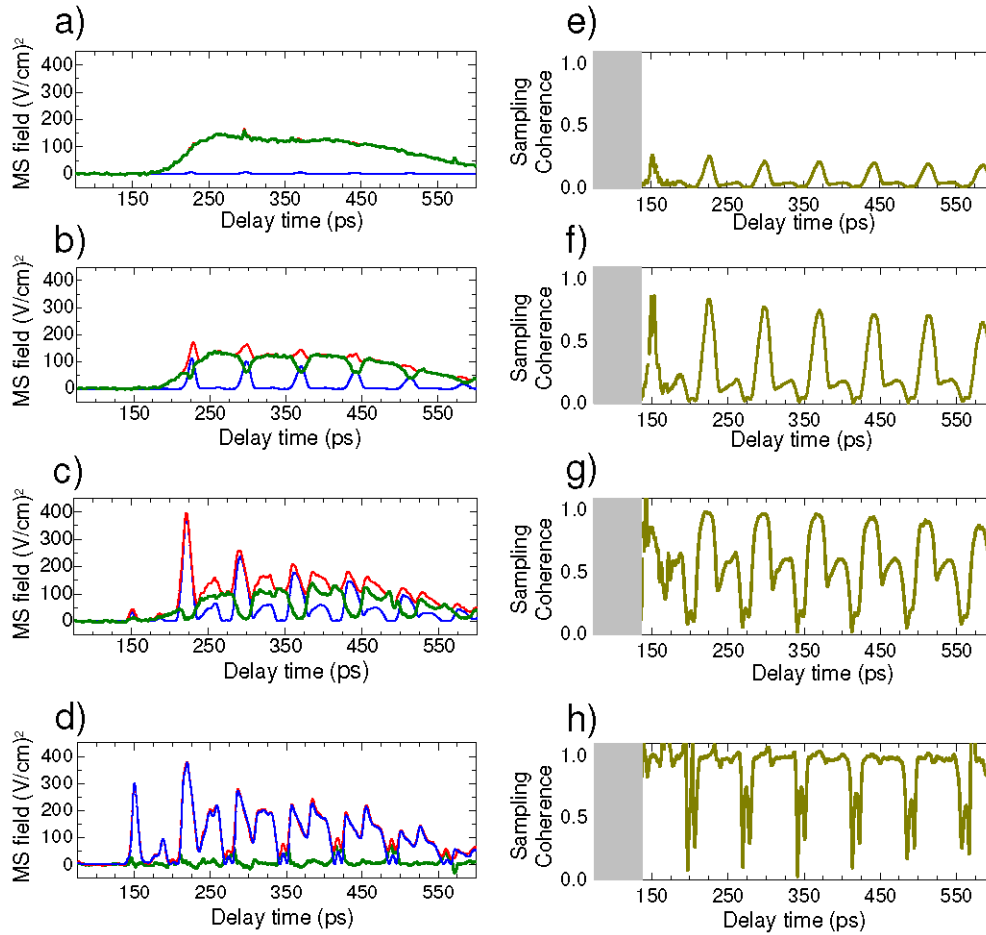


Fig. 3. **a-d**) Blue curves are the mean square (MS) synchronized field-envelope. Red curves are the total (synchronized and non-synchronized) MS field-envelope. The green curves are the MS non-synchronized field-envelope and are found by subtracting the MS field-envelope (blue curve) from the total MS field-envelope (red curve). The THz seed pulses are generated with photo-conductive antenna biases of **a)** 0.05V, **b)** 0.2V, **c)** 0.8V, and **d)** 4.0V. The amplitude of a THz seed pulse is proportional to the antenna bias. **e-h**) The degree of sampling coherence as a function of time for the corresponding curves in **a-d**). In the grey regions the sampling coherence is undefined since no THz field is present at these times. For all curves a quasi-DC bias of 1.91V ( $70 A/cm^2$ ) is applied to the QCL along with 6W of RF power.

## 5. Conclusion

Techniques are being developed to phase-lock THz QCLs for coherent detection, since such phase-locked QCL sources could have a major impact on far-infrared spectroscopy. However coherent detection is incapable of detecting non-synchronized radiation and the measured synchronized field may not be representative of the actual field. Although the degree of synchronization, i.e. the sampling coherence, of QCLs can be characterized with average power measurements; such methods assume the sampling coherence is constant in time. In the present work the sampling coherence of an injection seeded QCL was characterized on picosecond time scales. Electro-optic sampling in the cross-polarizer geometry enabled measurements of the instantaneous power emitted from the QCL. The sampling coherence

was found to be time dependent, illustrating the importance of time-resolved measurements. Besides verifying whether QCLs exhibit complete sampling coherence for all times, the dynamics of the phase-locking and synchronization process of QCLs could also be investigated. For example the response of the sampling coherence to an incoherent pump which de-synchronizes the QCL could be studied in the time domain.

### Appendix: Coherent and incoherent detection in the quarter-wave and cross-polarizer geometries

The THz field,  $E_{\text{THz}}(t)$ , induces a small birefringence,  $\Gamma(t)$ , between the principal axes of the electro-optic crystal which is transferred to the polarization state of the femtosecond sampling beam. The birefringence is proportional to the THz field,  $\Gamma(t) = \eta E_{\text{THz}}(t)$ , where  $\eta$  is a constant that depends on the crystal's length, electro-optic coefficient, index, and orientation. This neglects absorption, phase-matching effects, and the frequency dependence of the electro-optic coefficient. However the ZnTe crystal used in the present study is thin enough (200 $\mu\text{m}$ ) so that these effects can be neglected [25]. The strength of the electro-optic signal,  $EO_{\lambda/4}(t)$ , in the quarter-wave geometry is

$$EO_{\lambda/4}(t) = P_o \sin(\Gamma(\tau)) \propto P_o (\Gamma(\tau)) = P_o \eta E_{\text{THz}}(\tau). \quad (2)$$

In Eq. (2)  $P_o$  is power of the femtosecond sampling beam, and the small angle approximation is used. In the cross-polarizer geometry the strength of the detected electro-optic signal is

$$EO_{\text{cross}}(t) = P_o \sin^2(\Gamma(\tau) + \Gamma_o) \propto P_o \{ \eta^2 E_{\text{THz}}^2(\tau) + 2\eta \Gamma_o E_{\text{THz}}(\tau) \}. \quad (3)$$

In Eq. (3)  $\Gamma_o$  is the optical bias attributed to a residual birefringence in the ZnTe [24]. Terms that do not depend on  $\Gamma(t)$  are neglected, since the THz field is modulated for lock-in detection. In contrast to the quarter-wave geometry, the cross-polarizer signal contains two terms; an amplitude response,  $2\eta \Gamma_o E_{\text{THz}}(t)$ , and a square-intensity response,  $\eta^2 E_{\text{THz}}^2(t)$ . If only non-synchronized radiation is present, the varying phase will cause the amplitude term to average to zero. The cross-polarizer signal will then measure the mean square (MS) of the THz field-envelope, and can be used to measure the emitted power from a non-synchronized QCL [22, 23]. For synchronized radiation the amplitude response will often dominate since typically  $2\Gamma_o \gg \Gamma(\tau)$ . As a result electro-optic detection in the cross-polarizer geometry can be used as an alternative to the quarter-wave geometry for coherent detection [24].

By using the following described techniques, electro-optic sampling in the cross-polarizer geometry can function as an incoherent detector which is only sensitive to the total MS field-envelope. An antenna modulation technique can be applied to remove the amplitude response in the cross polarizer geometry. Applying an opposite voltage to the THz generating antenna creates an identical THz seed pulse with an opposite sign. The sign of the amplitude component can then be modulated without changing the value of the square-intensity component in Eq. (3). In theory this should enable lock-in detection to remove the amplitude response, and only measure the square response. In practice this reduces the amplitude response by a factor of  $\sim 200$ . To eliminate the residual amplitude component and the oscillation component of the square-intensity response a fast scan technique is employed. The optical delay line is scanned at a relatively fast speed of  $\sim 1\text{ps/second}$  (delay time/laboratory time) while using a long time constant (1 second) with a 24dB/octave roll-off filter. This averages out the residuals inusoidal oscillations. The fast-scan technique works since the slowly varying envelope approximation is valid for the QCL emission, i.e. changes in the pulse-envelope take place on a longer time scale than the field oscillations. Although the fast scan technique shifts the signal to later times (the data is shifted by  $\sim 4\text{ps}$ ), measurements at shorter and longer time constants show the shape of the MS-field envelope is not significantly affected. The antenna modulation and fast scan techniques permit electro-optic sampling in the cross polarizer geometry to only detect the MS field-envelope of the QCL emission.



The signal response of the separate detectors used for the cross-polarizer and quarter-wave geometry is calibrated using the data in Figs. 2(a) and 2(b). When laser action is initiated by spontaneous emission in Fig. 2(a), no laser emission occurs before 200ps. Any emission before 200ps arises from the THz seed and can be used to calibrate the cross-polarizer and quarter-wave geometry detector response.

### **Acknowledgments**

This work was supported by ANR projects “HI-TEQ” (ANR-09-NANO-017) and “THINQE-PINQE” (ANR-09-NANO-007) (France); ERC Advanced Grant projects NOTES, TOSCA, and EPSRC (UK); the Royal Society; and the Wolfson Foundation. MSMI acknowledges support from the MARA Agency, Government of Malaysia. N. J. acknowledges support from Referat 221 MIWF NRW.